

ULTRASENSITIVE TEMPERATURE SENSOR BASED ON FIBER-OPTIC FABRY-PÉROT INTERFEROMETER WITH VERNIER EFFECT

Yuqiang Yang,^{1,2} Yongguang Wang,² Yuxin Zhao,² and Jiuxing Jiang^{2*}

¹*Higher Educational Key Laboratory for Measuring and Control Technology
and Instrumentations of Heilongjiang Province
Harbin University of Science and Technology
Harbin 150080, China*

²*Institute of Photonics and Optical Fiber Technology
Harbin University of Science and Technology
Harbin 150080, China*

*Corresponding author e-mail: jjx_hrbust@sina.com

Abstract

We propose and demonstrate an ultrasensitive temperature sensor based on a fiber-optic Fabry-Pérot interferometer (FPI) with the Vernier effect. The sensor is prepared by splicing a section of silica tube and single-mode fiber (SMF) to a section of SMF in sequence, which formed two-cascaded FPIs. Their superimposed spectrum can produce the Vernier effect and form the interference spectrum envelope due to a similar free spectrum range (FSR). The shift of the interference spectrum envelope is much larger than that of a single FPI, when the temperature changes. Experimental results show that the designed sensor can provide a high temperature sensitivity of 183.99 pm/°C, which is almost 220 times higher than that of a single air cavity (0.86 pm/°C) and about 20 times higher than that of a single silica cavity (9.14 pm/°C). The sensor designed has compact structure (< 1 mm) and high sensitivity, providing a prospect for successful applications.

Keywords: fiber optic sensor, Fabry-Pérot interferometer, Vernier effect, temperature sensor.

1. Introduction

Optical fiber temperature sensors have been extensively studied over the last two decades due to the advantages of light weight, electrically passive operation, flexibility, long lifetime, and immunity to electromagnetic interference. A large number of such sensors have been developed based on different technologies, such as fiber-grating-based [1–6] and interferometer-based temperature sensors [7–10]. Among them, the air-gap microcavity based Fabry-Pérot interferometer (FPI) sensors are particularly attractive for temperature sensing due to their compact structure, small cross sensitivity, good stability, flexibility in tuning of sensitivity, and low cost. Thus, a variety of air-gap microcavity based FPI configurations has been proposed to measure temperature such as coating film [11, 12], chemical etching [13], micromachining [14], lateral offset splice [15], refractive index (RI) mismatch between two fiber splicing points [16–18], and so on. As we know, the temperature sensitivity of FPI using the fiber itself as a sensing part is low; further, using the sensitive material as the sensing part to enhance the sensitivity

will not only increase the complexity of production but is also limited by the material itself. Hence, a better method is needed to improve the sensitivity.

The Vernier effect is a very effective method to enhance the sensitivity of measuring devices. It is widely used in calipers and barometers. There are some structures that implement the Vernier effect today; in 2008, Rao [19] et al. proposed an intrinsic FPI with the Vernier effect formed by a section of endlessly single-mode photonic-crystal fiber (EPCF) and a single-mode fiber, which is expected to realize a low-cost and portable high-sensitivity temperature sensor. In 2015, Shao [20] et al. made a fiber-optic temperature sensor using two-cascaded Sagnac interferometers, with the sensitivity improved about 9 times. However, it is difficult to measure the temperature with high spatial resolution due to the large size of the sensor. In 2018, Lu [21] et al. demonstrated a fiber-optic temperature sensor based on two-cascaded FPIs with slightly different cavity lengths that considerably improved the sensitivity. The above review is sufficient to show that we can obtain higher temperature sensitivity by adjusting two cascade cavities with the Vernier effect.

In this paper, we propose a fiber temperature sensor based on FPI with the Vernier effect, which has compact structure and high sensitivity. The sensor is prepared by splicing several hundred micron silica tube and SMF to a section of SMF in sequence. Two cascaded FPIs with similar FSR are formed that produces the Vernier effect due to the slight optical path difference of the two interferometers. Furthermore, compared with the reported work where two Sagnac interferometers with slightly different FSRs were used [20] and four beams of light were reflected from the sensor head [21] to generate the Vernier effect, our sensor only employs three beams of light reflected from the two splicing joints and the cleaved SMF end face to achieve the Vernier effect. Hence, such a sensor is more compact than the previous ones to achieve the Vernier effect. Utilizing this feature to achieve temperature measurements of high sensitivity (about 183.99 pm/°C), the sensitivity increased three orders of magnitude compared with a single air-cavity FPI.

This paper is organized as follows.

In Sec. 2, we analyze the operation principle of the ultrasensitive temperature sensor based on fiber-optic Fabry–Pérot interferometer (FPI) with the Vernier effect and devote Sec. 3 to the sensor fabrication and experiments.

2. Operation Principle of the FPI Proposed

The configuration of the proposed ultrasensitive fiber-optic FPI temperature sensor is shown in Fig. 1. When the incident light in SMF, which serves as a lead-in fiber, travels to the reflecting mirrors M1, M2, and M3 in turn, part of the light will be reflected at the interface due to the refractive index (RI) mismatch. So M1 and M2 form an air cavity, denoted as FP1, with length L_1 . M2 and M3 form a silica cavity, denoted as FP2, with length L_2 .

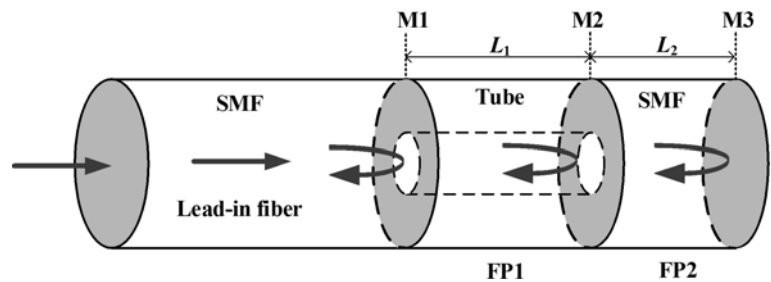


Fig. 1. Schematic of proposed cascaded FPIs.

The reflection spectrum of the air-cavity FP1, composed of M1 and M2, is typical double-beam interference. Assuming that the reflection coefficients of M1 and M2 are R_1 and R_2 respectively, the

reflection spectrum of the FP1 can be expressed by

$$I_r = A^2 + B^2 + 2AB \cos(2\phi_1), \quad (1)$$

where $A = \sqrt{R_1}$, $B = (1 - \alpha_1)(1 - R_1)\sqrt{R_2}$, α_1 is the transmission loss in mirror M1, $\phi_1 = 2\pi n_1 L_1 / \lambda$ is the phase shifts in the FP1, $n_1 = 1.0003$ is the RI of the air in the FP1, and λ is the wavelength of input light. If the condition $\phi_1 = 2\pi m$ (m is an integer and represents the fringe order) is fulfilled, the reflection spectrum will reach its maximum. Therefore, the dip wavelength of the m order is given by

$$\lambda_m = 2n_1 L_1 / m. \quad (2)$$

We can derive the FSR between the two adjacent dips as

$$FSR_1 = \lambda / 2n_1 L_1. \quad (3)$$

When the ambient temperature changes, both refractive index n_1 and cavity length L_1 are changed due to the thermo-optic effect and thermal expansion effect of the medium in the cavity. Then the temperature sensitivity of FP1 can be expressed as

$$S_1 = \frac{d\lambda_m}{dT} = \lambda_m \left(\frac{dL_1}{dT} \frac{1}{L_1} + \frac{dn_1}{dT} \frac{1}{n_1} \right), \quad (4)$$

where $\frac{dL_1}{dT}$ is the thermal expansion coefficient of silica of the FP1, equal to $5.5 \times 10^{-7} / ^\circ\text{C}$ [22], and $\frac{dn_1}{dT}$ is the thermo-optic coefficient of air of the FP1. Due to the fact that the RI of air is almost unchanged under changed temperatures in the range of a few hundred degrees Celsius, the influence of the air thermo-optic can be neglected. The calculated temperature sensitivity of the FP1 is $0.85 \text{ pm}/^\circ\text{C}$ at $1,550 \text{ nm}$, which explains why the air-filled cavity is thermally insensitive, whereas the thermo-optic coefficient of silica is $8.5 \times 10^{-6} / ^\circ\text{C}$ [23], and the calculated temperature of the silica-cavity FP2 is $9.94 \text{ pm}/^\circ\text{C}$ at $1,550 \text{ nm}$. As we can see, the temperature sensitivity of the silica cavity is more than ten times higher than that of an air cavity. Hence, the Vernier effect is introduced in order to improve the sensitivity of the sensor. We should guarantee the FSR of FP1 and FP2 to be very close but not equal by cutting the SMF on the other end of the silica tube into L_2 length. The double cavities will produce the Vernier effect and then the lower frequency interference spectrum envelope. The FSR of this envelope is determined by the FSR of FP1 and FP2; it reads

$$FSR_{\text{envelope}} = M \times FSR_2, \quad (5)$$

where $FSR_2 = \lambda / 2n_2 L_2$ is the FSR of FP2, and M is the amplification factor, which can be expressed by

$$M = \frac{FSR_1}{|FSR_1 - FSR_2|}. \quad (6)$$

The change in ambient temperature results in the frequency shift of the dual-cavity interference spectrum envelope, so the temperature sensitivity of the envelope can be expressed as

$$S_2 = \frac{d\lambda_{\text{envelope}}}{dT} = M \times \lambda_m \left(\frac{dL_2}{dT} \frac{1}{L_2} + \frac{dn_2}{dT} \frac{1}{n_2} \right), \quad (7)$$

where $\frac{dL_2}{dT}$ and $\frac{dn_2}{dT}$ are the thermal expansion coefficient and thermo-optic coefficient of FP2, respectively. This shows that the frequency shift of the dual-cavity interference spectrum envelope is M times larger than that of a single cavity; compare with Eq. (4).

Using the above equations, we simulated the output of FP1 and FP2 and the output of the cascaded dual cavity; the results are shown in Fig. 2, where L_1 and L_2 are set to be 344.98 and 227.02 μm , respectively. From Fig. 2a and b, we can see that the shift of the spectral valley of FP2 (0.64 nm) is larger than that of FP1 (0.06 nm), and the corresponding temperature sensitivities are 9.14 pm/ $^{\circ}\text{C}$ and 0.86 pm/ $^{\circ}\text{C}$, respectively. Figure 2c obviously shows that the envelope curve drift in the direction of short wavelength is about 13.37 nm, and the temperature sensitivity is about 191.03 pm/ $^{\circ}\text{C}$. The temperature sensitivity increases more than 220 times in comparison with the single air-cavity FP1. Therefore, the simulation results demonstrate that the application of Vernier effect demodulation is an effective method to improve the sensitivity of temperature-sensitive measurements.

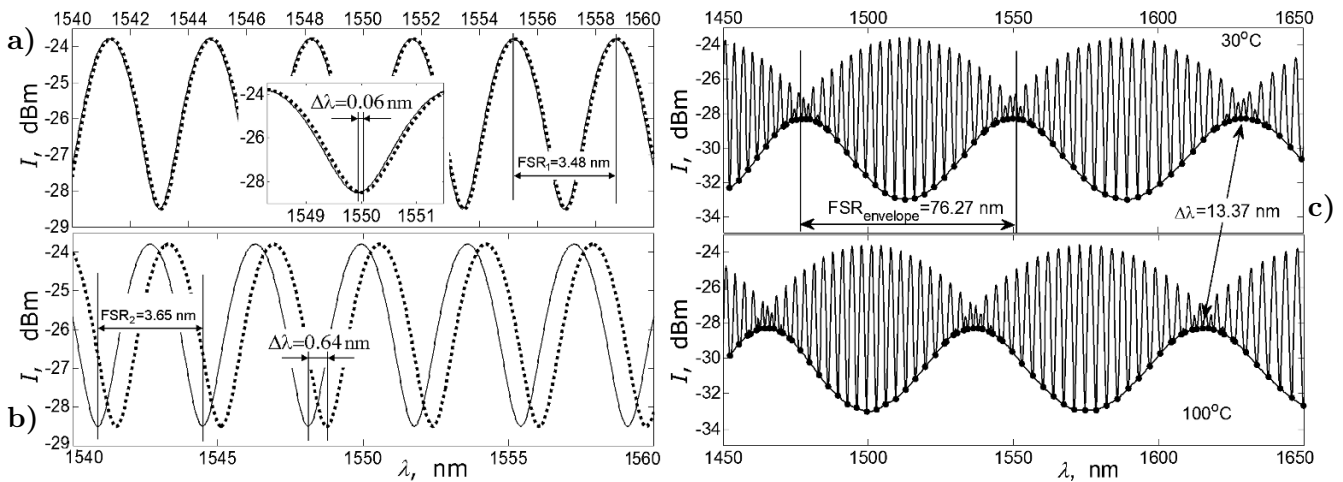


Fig. 2. Simulated temperature responses of the FPI based on a single air cavity FP1 (a), silica cavity FP2 (b) (solid curves correspond to 30°C and dotted curves correspond to 100°C), and cascaded dual cavity (c).

3. Sensor Fabrication and Experiments

A schematic diagram of the experimental setup is shown in Fig. 3. It consists of a broadband light source (BBS) and an optical spectral analyzer (OSA, Yokogawa AQ6370C) with a resolution of 0.02 nm. The sensors are placed in an adjustable temperature control oven, and the temperature in the experiment changes from 38°C to 100°C with an interval of 6°C. The fabrication process of the temperature sensor is as follows: First, a section of silica tube is spliced to the cleaved end of a section of SMF, which serves as a

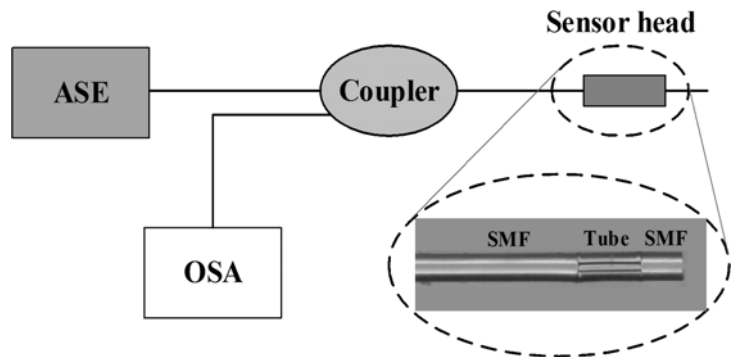


Fig. 3. Schematic diagram of temperature sensing experimental setup.

lead-in fiber. Second, the tube is cleaved to a designed length. Finally, another section of cleaved SMF is spliced to the cleaved endface of the tube. The two joints were spliced automatically with a commercial electric arc fusion splicer (Fujikura 80S). A microscope photograph of the fabricated sensor is shown in the inset in Fig. 3. The geometric lengths of the FP1 and FP2 are about 344.98 and 227.02 μm , respectively. The corresponding reflection spectrum for the cavity at room temperature is shown in Fig. 4 a; here, FSR is about 72 nm, which is basically consistent with the simulation results.

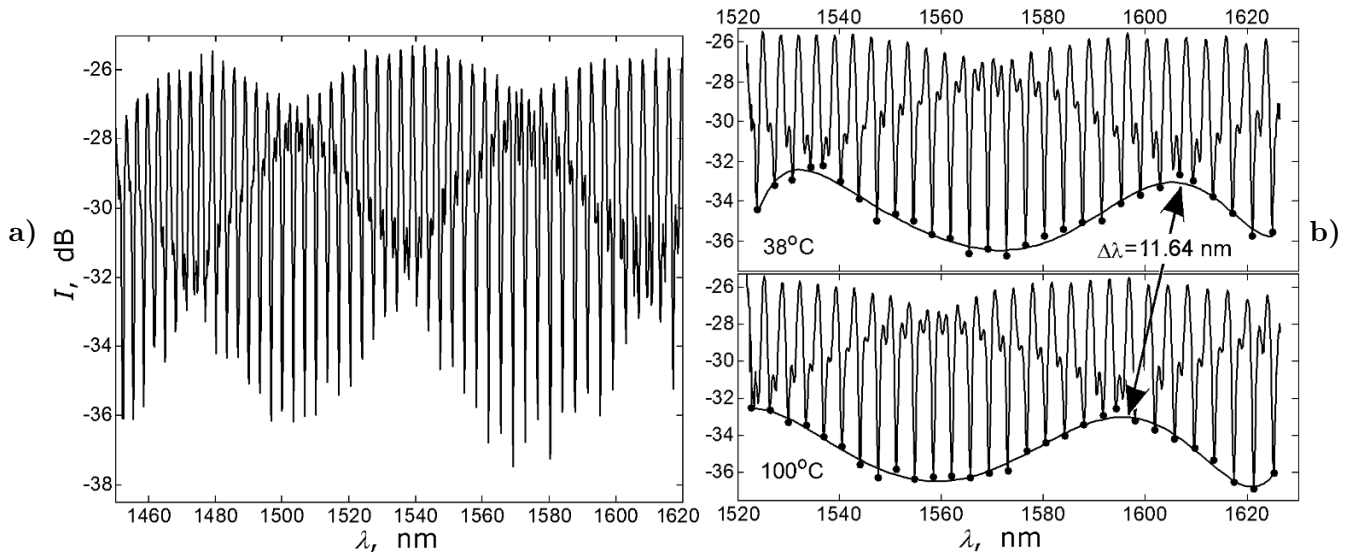


Fig. 4. Reflection spectrum of the proposed sensor at room temperature (a) and its changes with temperature (b).

Figure 4 shows the interference spectrum temperature characteristic of the cascaded dual-cavity with the Vernier effect (inset in Fig. 3). We can see that the envelope curve was significantly shifted in the short-wavelength direction (about 11.64 nm) with increase in temperature. Figure 5 illustrates the center wavelength of the wave valley of the envelope curve moving with the temperature at different temperatures. One can see that the center wavelength shifts linearly with the ambient temperature with $R^2 = 0.9981$, and the temperature sensitivity is 183.99 pm/°C, which is basically consistent with the simulation results. The sensitivity is almost 220 times higher than that in the single air cavity and about 20 times higher than that in the single silica cavity. So, we can obtain different degree of magnification by adjusting the length of the FP2 to suit different applications.

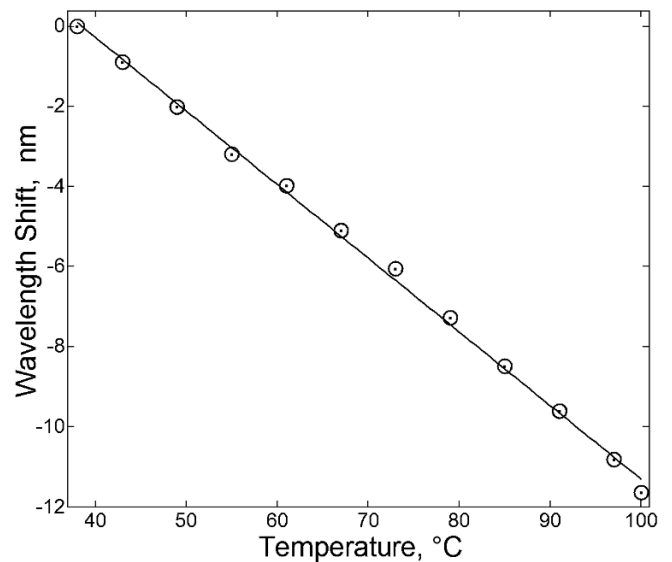


Fig. 5. Wavelength shifts of the proposed sensor versus the temperature.

4. Summary

In summary, we proposed, designed, and demonstrated a compact and simple temperature sensor based on a fiber-optic Fabry–Pérot interferometer with the Vernier effect. The sensor is prepared by splicing a section of silica tube and SMF to a section of SMF in sequence, which formed two cascaded FPIs. Accurate control of the length of the silica tube and the SMF on the other end ensures that the two interferometers have similar FSR, so the superposition spectrum produces the Vernier effect. We tested experimentally the temperature response characteristics of the sensor elaborated. The sensitivity of the cascaded dual cavity with the Vernier effect is $183.99 \text{ pm}/^\circ\text{C}$, which is almost 220 times higher than that of the single air cavity ($0.86 \text{ pm}/^\circ\text{C}$) and about 20 times higher than that of the single silica cavity ($9.14 \text{ pm}/^\circ\text{C}$). The results obtained show that this method is an effective way to improve the sensitivity of the sensor. In addition, the sensor has compact structure and high sensitivity and can be used in industrial production, as well as biomedical and other temperature detection fields.

Acknowledgments

The authors acknowledge the financial support provided within the National Natural Science Foundation of China under Projects Nos. 51777046, 51672062, and 51575149 and the Natural Science Foundation of Heilongjiang Province under Project No. F2017012.

References

1. T. L. Lowder, K. H. Smith, B. L. Ipson, et al., *IEEE Photon. Tech. L.*, **17**, 1926 (2005).
2. C. M. Jewart, Q. Q. Wang, J. Canning, et al., *Opt. Lett.*, **35**, 1443 (2010).
3. H. Q. Li, H. J. Yang, E. B. Li, et al., *Opt. Express*, **20**, 11740 (2012).
4. T. G. Liu, Y. F. Chen, Q. Han, et al., *Appl. Opt.*, **55**, 791 (2016).
5. T. Chen, R. Z. Chen, C. Jewart, et al., *Opt. Lett.*, **36**, 3542 (2011).
6. R. Subramanian, C. Zhu, H. Zhao, et al., *IEEE Photon. Tech. L.*, **30**, 327 (2018).
7. Y. Cui, P. P. Shum, D. J. J. Hu, et al., *IEEE Photon. J.*, **4**, 1801 (2012).
8. H. Liao, P. Lu, X. Fu, et al., *Opt. Express*, **25**, 26898 (2017).
9. X. Tan, Y. Geng, X. Li, et al., *Appl. Opt.*, **52**, 8195 (2013).
10. W. Ni, P. Lu, X. Fu, et al., *Opt. Express*, **26**, 18341 (2018).
11. C. Li, Q. Liu, X. Peng, et al., *Opt. Express*, **23**, 27494 (2015).
12. S. Liu, Y. Ji, J. Yang, et al., *Sens. Actuators A*, **269**, 313 (2018).
13. W. Zheng, J. Xie, Y. Li, et al., *Opt. Commun.*, **324**, 234 (2014).
14. Y. Zhang, L. Yuan, X. Lan, et al., *Opt. Lett.*, **38**, 4609 (2013).
15. Y. Wu, Y. Zhang, J. Wu, et al., *J. Lightwave Technol.*, **35**, 4311 (2017).
16. C. Chan, H. Su, J. Yang, et al., *Opt. Express*, **23**, 17687 (2015).
17. H. Yu, Y. Wang, J. Ma, et al., *Sensors*, **18**, 273 (2018).
18. B. Xu, Y. Yang, A. Jia, et al., *Opt. Express*, **25**, 14483 (2017).
19. Y. J. Rao, M. Deng, D. W. Duan, et al., *Sens. Actuators A*, **148**, 33 (2008).
20. L. Y. Shao, Y. Luo, Z. Zhang, et al., *Opt. Commun.*, **336**, 73 (2015).
21. J. Zhang, L. Hao, P. Lu, et al., *IEEE Photon. J.*, **10**, 1109 (2018).
22. Y. F. Wu, Y. D. Zhang, J. Wu, et al., *J. Lightwave Technol.*, **35**, 4311 (2017).
23. J. Komma, C. Schwarz, G. Hofmann, et al. *Appl. Phys. Lett.*, **101**, 041905 (2012).